Tectonophysics, 166 (1989) 293–315
Elsevier Science Publishers B.V., Amsterdam – Printed in The Netherlands

Doming mechanisms and structural development of two domes in Ramon, southern Israel

GIDON BAER [1] and ZE'EV RECHES [2]

[1] *Geological Survey of Israel, 30 Malkhe Israel St., Jerusalem 95501 (Israel)*
[2] *Department of Geology, Hebrew University, Jerusalem 91904 (Israel)*

(Received April 18, 1988; accepted December 15, 1988)

Abstract

Baer, G. and Reches, Z., 1989. Doming mechanisms and structural development of two domes in Ramon, southern Israel. *Tectonophysics*, 166: 293–315.

Domes may develop above igneous intrusions, over rising diapirs, along strike-slip faults or within arrays of folds. The details of doming mechanisms are resolved here for two domes in southern Israel by determining and modeling the tectonic paleostresses. These domes are elongated structures with width to length ratios of 1 : 2, developed in Triassic and Jurassic sedimentary layers. The domes are adjacent and parallel to the Ramon fault, which is part of a 250 km long and 50 km wide shear zone. A quartz-syenite body of Early Cretaceous age intruded one of the two domes, Gevanim. This intrusion has a stepped geometry in cross section, in which concordant roof segments are connected by vertical piercement faults; some of these faults are continuous into the overlying sedimentary layers. The second dome, Saharonim, has no central intrusion.

The paleostress field within and outside the domes was determined by stress inversion of fault-slip data and by dynamic analysis of calcite twins. The two domes differ in their stress history and doming mechanisms. The Gevanim Dome initiated according to Gilbert's model of laccolithic intrusion: uplift and bending associated with the emplacement of the quartz-syenite body along peripheral faults. The stress field during the intrusive stage was of vertical σ_1, radial σ_2 and tangential σ_3. The Saharonim Dome initiated during the Triassic as a tilted block, and developed into a dome under layer-parallel compression since the Late Cretaceous. The two domes were later amplified by the regional stress fields of Late Cretaceous to Recent. It is likely that stress rotation associated with slip along the Ramon fault affected the development of the domes.

Introduction

The development of domal structures in sedimentary rocks has been studied since Gilbert proposed his laccolith model in 1877. Three basic types of domes may be distinguished. The first type includes domes that form by layer-parallel compression. Johnson and Page (1976) termed such domes double-plunging folds and demonstrated a continuous transition from a circular dome to an elongate dome to a non-plunging fold. They showed that the ratio of the length of the two axes of an elongated dome is related to the ratio of the principal stresses which form the dome.

Domes are also associated with strike-slip faults; they usually occur at the vicinity of steps and bends along these faults (Segall and Pollard, 1980; Reches, 1987a). Such domes are common along the San Andreas system (Segall and Pollard, 1980), the Dead Sea rift (Freund, 1965) and the Sinai–Negev shear zone (Bartov, 1974). These domes are thought to form in response to horizontal compression associated with the local irregularities of the fault surface. Segall and Pollard (1980) calculated the stress fields associated with seg-

0040-1951/89/$03.50

mented strike-slip faults. They showed that the mean compressive stress and the shear stresses increase between the two segments of the fault, and that the regional principal stress axes are rotated by as much as 15° in these regions. Zoback et al. (1987) suggested a different doming mechanism along strike-slip faults. They compiled the state of stress for the San Andreas fault system and found that at distances of 100 km or more from the fault, the axis of the maximum horizontal compressive stress lies at an angle of about 50° to the strike of the fault. Closer to the San Andreas fault, however, this stress axis is perpendicular to the fault trend. Zoback et al. (1987) proposed that the stress rotates due to the low strength of the fault zone, and that the rotated stress is the cause for the many folds and elongated domes which parallel the San Andreas fault.

Domes may also develop by bending in response to the rise of a diapir or the emplacement of an igneous intrusion. The igneous domes in the Henry Mountains, Utah are typical examples of such structures (Gilbert, 1877; Hunt, 1953; Pollard and Johnson, 1973; Jackson and Pollard, 1988). The domes in the southern Henry mountains are circular in plan view. Inclined layers encircle the central igneous body and the sedimentary rocks are cut by radial and tangential fault systems (Jackson, 1987).

Doming of the third type may be detected by ground surface deformation in regions of volcanic activity. This deformation is closely related to the upward movement of magma under the volcanic edifice. Mogi (1958) modeled the observed vertical displacement on ground surface by a small, inflating source within an elastic half space. Dieterich and Decker (1975) expanded Mogi's analysis to include various reservoir geometries and strain conditions. They showed that the geometry of the deep igneous body and the strain conditions can be deduced from the observed surface displacements.

Each of the three doming mechanisms mentioned above, has a distinctive state of stress associated with it. Identification of these stress states is essential for the understanding of the doming style (for example, Withjack and Scheiner, 1982; Jackson, 1987).

We present here a study of two domes, Gevanim and Saharonim, in the Ramon area of southern Israel (Fig. 1). The structure of the domes, the dominant fault patterns and the geometry of a central intrusion is described first. Then, we use the new stress inversion method of Reches (1987b) to calculate the stress tensors within and around the domes. An analytical model for stress distribution in an uplifted dome is derived and compared with the observed structure and calculated stresses.

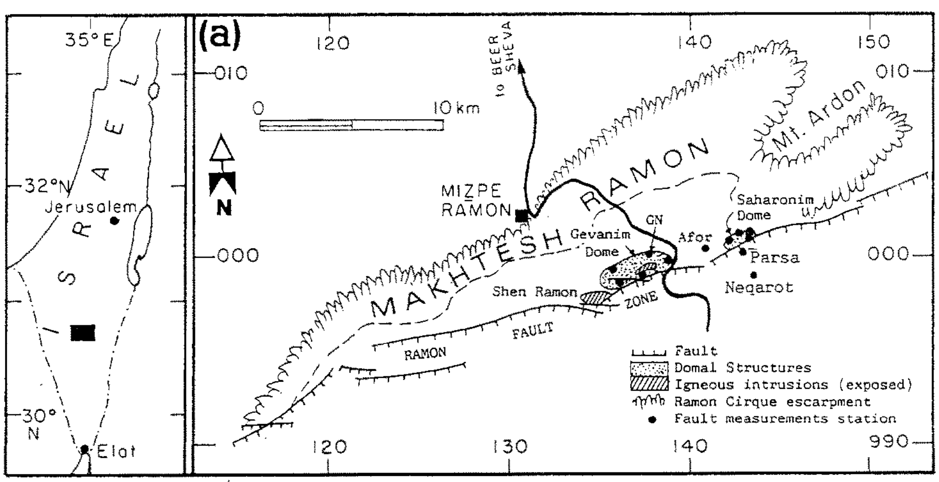

Fig. 1. Location maps of the Ramon domes (geology after Zak, 1968). a. Regional setting. b. Geological map and fault stations in Gevanim dome. c. Geological map and fault stations in Saharomin dome. Names of stations are: *GS*—Gevanim South, *GE*—Gevanim East, *GN*—Gevanim North, *GNW*—Gevanim Northwest, *SSE*—Saharonim Southeast, *SNE*—Saharonim Northeast, *SN*—Saharonim North, *SW*—Saharonim West, *AF*—Afor, *PA*—Parsa, *NEQ*—Neqarot.

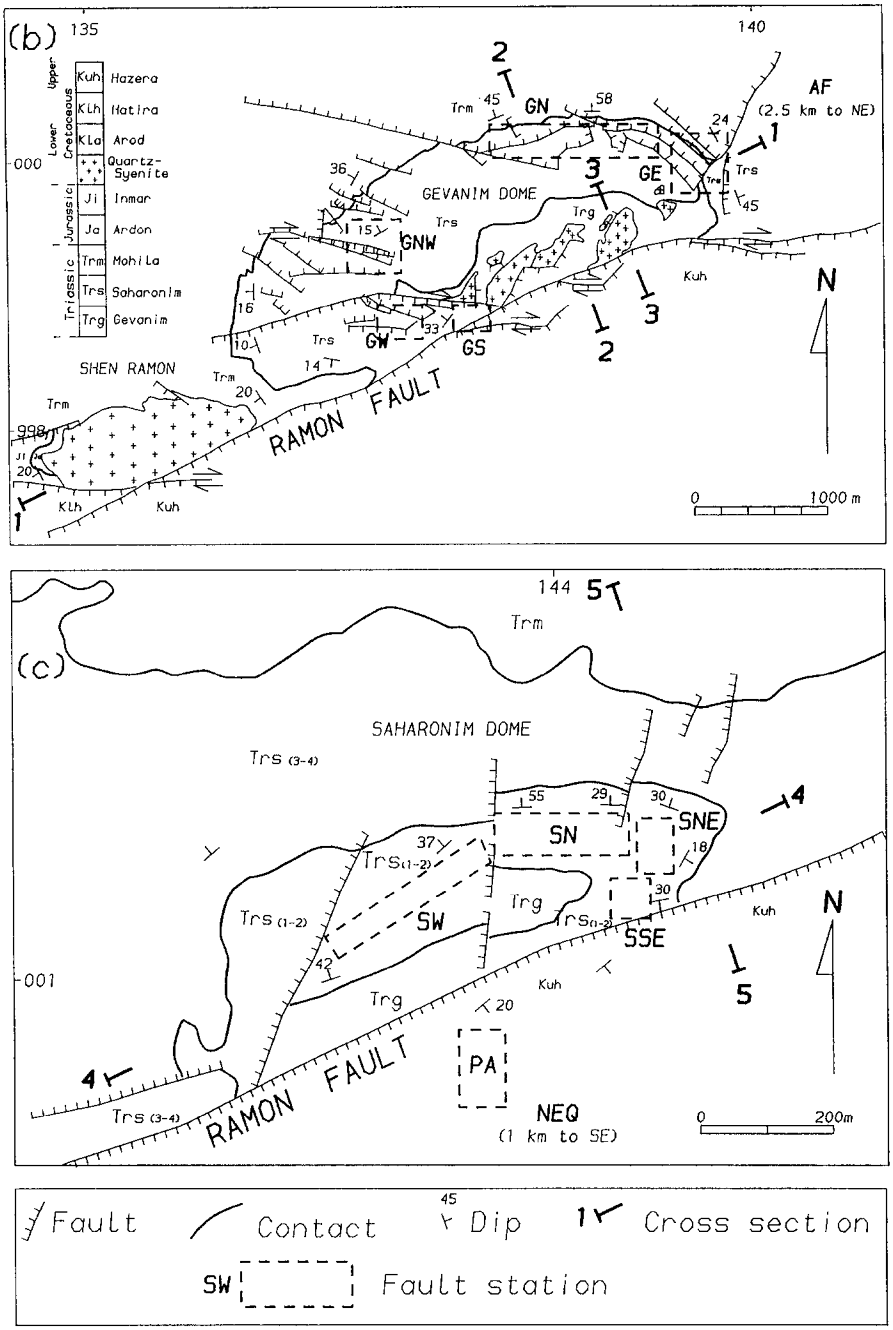

Fig. 1 (continued).

Finally, the development of the domes is reconstructed with respect to prevailing regional stresses during the doming.

The Ramon domes

The two studied domes, Gevanim and Saharonim, are part of the Ramon anticline in southern Israel (Fig. 1). The erosion into the deep structural levels of the domes, the good exposures of sedimentary layers and intrusive rocks, the numerous faults with slip indicators and the moderate deformation of the host rocks, make the two domes in Ramon, an excellent site for domal investigations. Further, the Gevanim Dome was intruded by a large quartz-syenite body; the surface and subsurface geometry of this intrusion is well known (Baer et al., 1985; Goldman et al., 1988). On the other hand, the Saharonim Dome was not intruded by a central igneous body. Thus, a study of these domes, can reveal the influence of a central intrusion.

Tectonic setting

The Ramon domes are bound on the south by the Ramon fault zone, which is in the eastern part of the 250 km long Sinai–Negev shear zone (fig. 1, in Bartov, 1974). The Ramon fault zone trends N70°E and it includes a major dextral oblique-slip fault with maximum vertical and horizontal displacements of 700 m and 2.5 km respectively, and accompanying folded and faulted structures (Garfunkel, 1964; Bartov, 1974).

Several post-Early Triassic tectonic phases have been identified in Ramon. The oldest phase was recognized by thickness changes, facial variations and unconformities observed in Triassic rocks in the eastern Ramon (Zak, 1957). These features are not related to the Ramon fault and are similar in character to stratigraphic evidence found in subsurface analysis of the eastern Mediterranean (Garfunkel and Derin, 1985).

A Late Triassic and Early Jurassic phase was recognized by an erosional unconformity of Lower Jurassic rocks over Upper Triassic units and by thickness variations of Lower Jurassic units (Garfunkel, 1964). As the magnitude of this unconformity increased toward the Ramon fault, Garfunkel (1964) suggested that the fault could have been active at that period. Freund et al. (1975) suggested that regional formation of basins during Triassic and Jurassic times was controlled by normal extensional faulting, and that the Ramon fault also acted as a normal one.

The Late Jurassic and Early Cretaceous times were dominated by regional magmatism. In the Ramon, a radial dike system was emplaced (Zak, 1957; Baer and Reches, 1987), thus suggesting that an isotropic state of stress prevailed at that time (Baer, 1989). The intrusive phase was followed by a regional uplift and intensive erosion, and by extrusive volcanism.

The next tectonic phase was initiated in the Late Turonian and has continued intermittently until Recent. It includes several periods of activity along the Ramon fault, as well as the development of open folds, monoclines and faults in Ramon and the entire Sinai–Israel subplate (Bentor and Vroman, 1951; De Sitter, 1962). Two different stress fields which are associated with this phase, have been determined from mesostructures by Eyal and Reches (1983). The older field of Late Turonian to Early Miocene age has a principal compressive axis trending N70°W; it is designated as the Syrian Arc stress. The younger field of Middle Miocene to Recent age, prevailed primarily in the vicinity of the Dead Sea transform, and it has a principal compressive axis trending N10°W; it is designated as the Dead Sea stress.

Slip occurred along the Ramon fault in the Late Turonian to Senonian time and after the Early Miocene (Garfunkel, 1964, Bartov, 1974). However, the concentration of deformation close to the Ramon line since the Triassic, suggests that the fault may have been active before the Turonian (Garfunkel, 1964, Freund et al., 1975).

Structure of Gevanim Dome

The Gevanim Dome is an elliptical structure that trends N70°E (Fig. 1b) with maximum exposed dimensions of 4 by 2 km and vertical uplift of about 400 m (Zak, 1968). The oldest exposed rocks are quartzitic sandstones of the Lower Triassic Gevanim Formation and the youngest rocks are carbonates and evaporates of the Middle Triassic Saharonim and Mohila formations (Fig. 1b). Dips vary around the dome (Fig. 1b). They are 15°–45° in the east limb, 20°–70° in the north, 5°–40° in the northwest, 5°–20° in the west and 20°–60° in the southern limb. Local, steeper dips are associated with drag along faults.

A fault belt 200–300 m wide encircles the margins of the dome (Fig. 1b). In the eastern and northern limbs this belt includes tangential reverse faults dipping 25°–80° westward and southward respectively and radial normal faults. In the northwestern, western and southern limbs, this belt is composed of several vertical strike-slip faults and normal faults.

Two fault systems traverse the center of the dome (Fig. 1b). The first system strikes E–W and is composed of strike-slip faults (Zak, 1957); the second system strikes N–S to N20°E and is dominated by dip-slip faults. A 500–700 m wide zone with no faults, separates the circumferential fault belt from the center of the dome (Fig. 1b).

Gevanim and Shen Ramon intrusions

A quartz-syenite intrusion and several associated sills and dikes, intruded the Triassic rocks in the central part of the Gevanim Dome. This intrusion has been studied in detail following the discovery of polymetallic mineralization at its upper contact (Itamar, 1987). The results of 30 drillholes, up to 100 m deep, and a Time Domain Electromagnetic survey (TDEM) were utilized to define the geometry of this intrusion (Baer et al., 1985; Goldman et al., 1988).

The larger quartz-syenite body of Shen Ramon intruded Upper Triassic and Lower Jurassic layers about 2 km southwest of the Gevanim Dome (Bentor, 1952) (Fig. 1b). Subsurface connection between the Gevanim and the Shen Ramon intrusions which was suggested by Bentor (1952) and Mazor (1955), has been recently confirmed by the TDEM survey (Goldman et al., 1988). This survey indicates that an igneous body extends at a depth of 50 to 200 m below the surface between the Shen Ramon and Gevanim intrusions. This extension roughly coincides with the outline of the Gevanim Dome (Fig. 2).

Absolute dating of the Shen Ramon and Gevanim intrusions yield similar K–Ar ages of 131 ± 3 Ma (Lang and Steinitz, 1985) and recent Rb–Sr dating of the Gevanim intrusion (Lang et al., 1988) yield an age of 124 ± 13 Ma; however, some observations indicate that they formed in the course of more than one event. First, the two intrusions have opposite paleomagnetic polarization (Ron and Baer, 1988), and second, intrusive contacts were found between two separable variants of quartz-syenite within the igneous body of Gevanim.

The geometry of the Gevanim intrusion was not known in detail until recently. Bentor (1952) initially described sills, and later termed them "ridges" (Bentor, 1963) because of their flat concordant roofs and discordant walls. Mazor (1955) suggested that the intrusion is composed of separate bosses, and Zak (1957, 1968) proposed that the intrusion is a single discordant boss which separated into blocks by later faulting. The recent surveys provided essential details. The drilling into the western and central parts of the intrusion (Baer et al., 1985) show that the thickness of the quartz-syenite body is at least 100 m, where the rock texture becomes equigranular plutonic; the

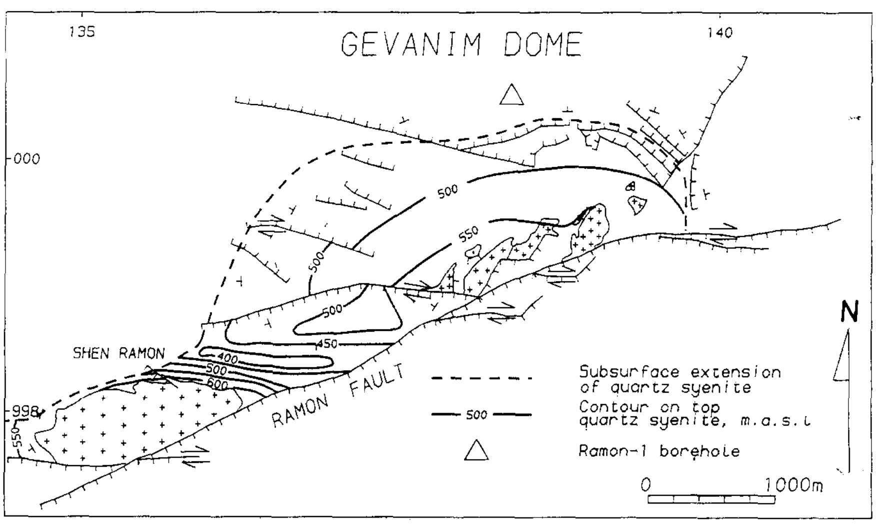

Fig. 2. Structural map on top of the quartz-syenite intrusion, southern Ramon (after the Time Domain Electromagnetic survey of Goldman et al., 1988). Minor faults were omitted.

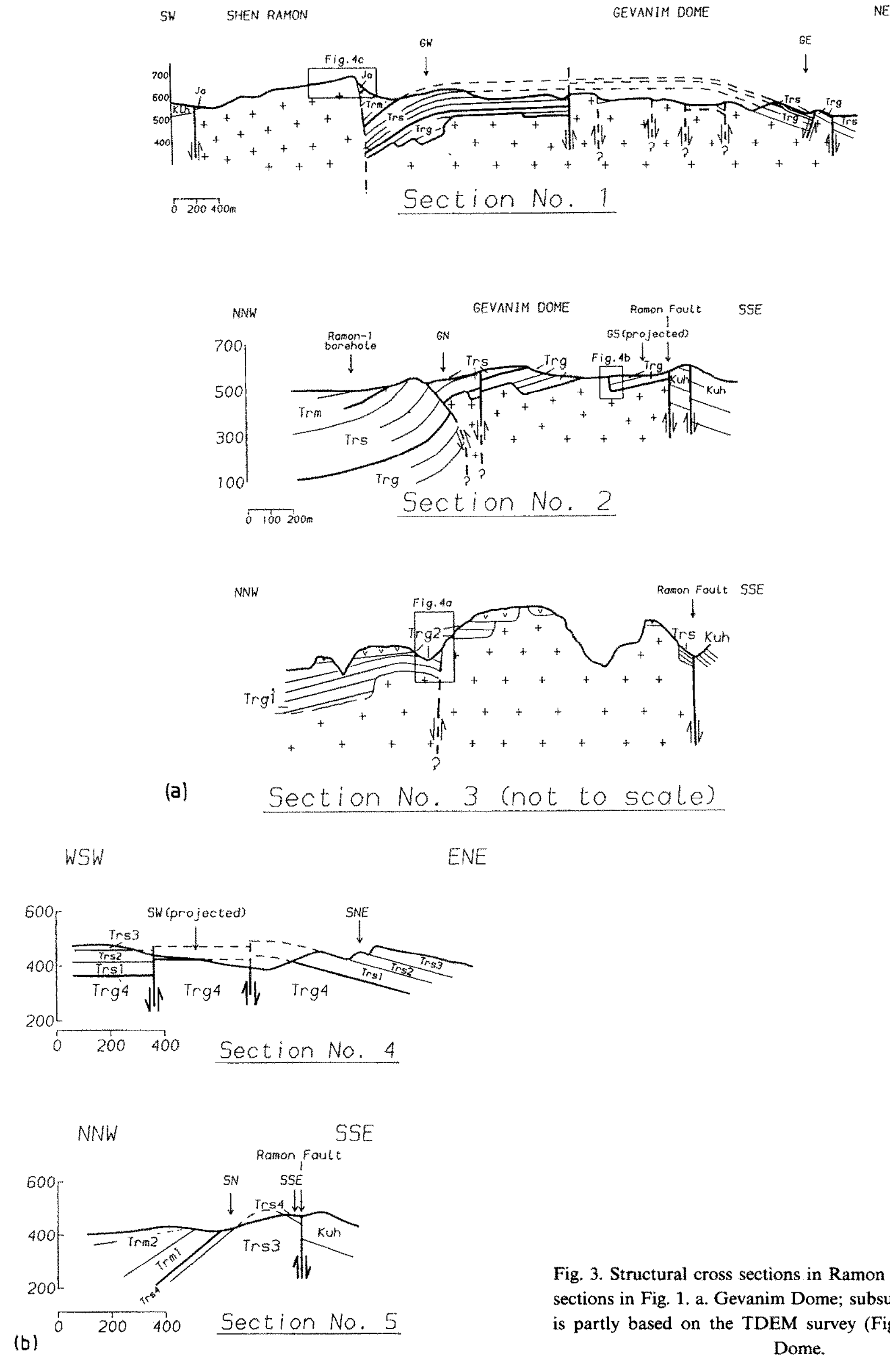

Fig. 3. Structural cross sections in Ramon domes. Location of sections in Fig. 1. a. Gevanim Dome; subsurface interpretation is partly based on the TDEM survey (Fig. 2). b. Saharonim Dome.

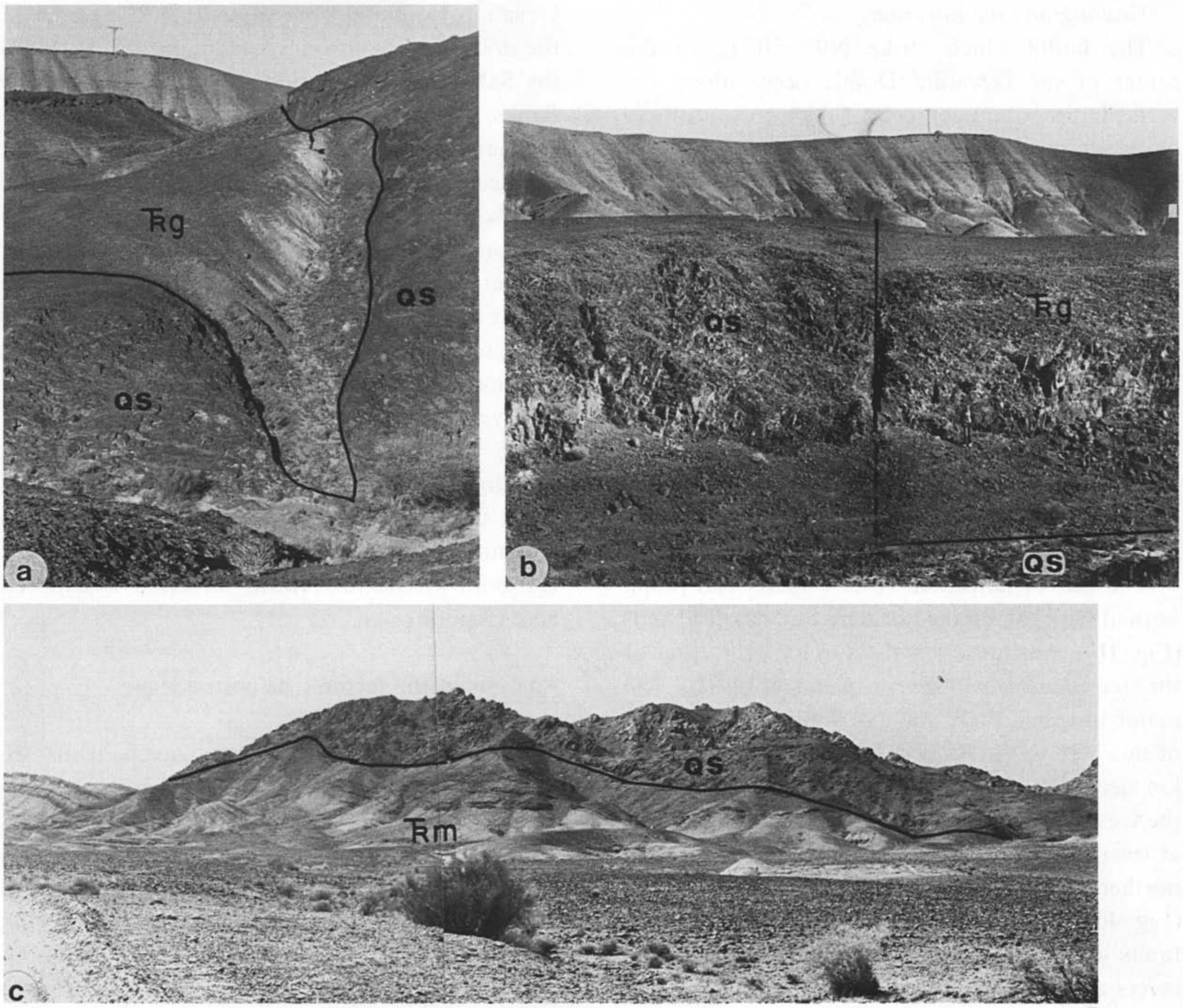

Fig. 4. Photographs of contacts between quartz-syenite bodies and Triassic sedimentary rocks in Ramon. QS-quartz-syenite; TRg and TRm are Gevanim and Mohila Formations. a. Quartz-syenite on the right side is in discordant, vertical contact with the sedimentary rocks in the center, whereas the quartz-syenite at the bottom left, is concordant to the overlying sedimentary rocks. Gevanium dome, location in section 3 of Fig. 3a. b. Concordant contact, at the bottom right, and piercement fault, in the center. Gevanim dome, location in section 2, Fig. 3a. c. The eastern, discordant contact between quartz-syenite and sedimentary rocks in Shen Ramon. Location in section 1, Fig. 3a.

TDEM survey indicates that this central intrusion extends far beyond the exposed outcrops.

The Gevanim and Shen Ramon intrusions have elliptical shape in map view, with their long axes trending parallel to the Ramon fault. The width to length ratio of the intrusion is between 1 : 4 and 1 : 3 (Fig. 1b). The roof of the intrusion in the Gevanim Dome is almost always concordant with the sedimentary layers. Locally, the roof climbs from one stratigraphic level to the other along vertical surfaces, which vary in height from a few meters to more than 50 m and generate a "stepped" geometry (Figs. 3a, 4). The intrusion reached different stratigraphic units: older layers at the center and younger layers at the margins (Fig. 3a). In Shen Ramon, the eastern and northern contacts are discordant, vertical surfaces, whereas the western contacts are concordant with the Ardon Formation (Fig. 3a).

Faulting and the intrusion

The faults which strike N0°–20°E, in the center of the Gevanim Dome, occur along the vertical, discordant contacts of the intrusion; these faults are restricted to the margins of the igneous outcrops (Figs. 1b, 3a, 4). In many locations, the roof of the intrusion does not attain the same stratigraphic level on both sides of these faults (section 3 in Fig. 3a). Therefore, we regard these faults as *piercement faults* along which the intrusion climbed into different levels in the sedimentary rocks.

The E–W striking faults in the center of the dome, and faults striking WNW in the western part of the dome, are strike-slip faults. In places they are accompanied by dikes, and they are not restricted to the margins of the central intrusion.

The belt of tangential reverse faults and radial normal faults along the northern and eastern limbs (Fig. 1b), coincides with the surface projection of the termination of the intrusion (Fig. 2). The major intrusive body was not found 300 m north of this belt, in the Ramon-1 borehole, which is 3.4 km deep. Therefore, the buried northern wall of the Gevanim intrusion must be discordant and dip at least 85° to the north, similarly to the exposed northern and eastern contacts of Shen Ramon (Fig. 4c). Zak (1957) suggested that the tangential faults were normal faults, formed by uplift of the layers around the intrusion. However, field evidence indicates that these are reverse faults which dip southward. These faults are apparently the upward continuation of the northern and eastern walls of the intrusion (Fig. 3a, section No. 2), and are therefore regarded as peripheral piercement faults.

The above descriptions indicate that an important deformation mechanism in the Shen Ramon and Gevanim intrusions is the piercement along vertical faults. The second deformation mechanism, the arching of the strata above the intrusion, will be discussed later in this paper.

Structure of the Saharonim Dome

The Saharonim Dome is an elongated structure trending N70°E with exposed dimensions of 1 by 0.5 km (Fig. 1c). Shales and limestones of the Gevanim Formation are exposed in the center of the dome and limestones, dolomites and shales of the Saharonim Formation are exposed along the flanks. The layers dip 30°–45° in the northwestern limb, 25°–65° in the north, 15°–35° in the northeast and 15°–30° in the southeastern limb. The southern part of the dome is cut by the Ramon fault (Fig. 3b). An angular unconformity of Late Triassic age appears northeast of the Saharonim Dome (Zak, 1957). The unconformity increases from the north towards the dome and may locally exceed 24° (section 5 in Fig. 3b).

Several strike-slip faults which trend N5°–20°E, traverse the Saharonim Dome (Fig. 1c). The dome is also crossed by two basaltic dikes of Early Cretaceous age and the sedimentary strata are intruded by a few basaltic sills. Unlike the Gevanim Dome no central intrusion is exposed here (Fig. 3b).

Analysis of the tectonic paleostresses

To evaluate the doming mechanisms in Gevanim and Saharonim structures, we determined the local paleostresses at nine stations within the domes and at three stations outside the domes. Two methods were used to calculate the paleostresses: (a) a new stress inversion method for fault slip data which incorporates failure conditions and calculates the magnitudes and orientations of the stress tensor (Reches, 1987b). This method provides the possibility to identify two (or more) phases of deformation in a group of faults measured at one site. (b) Dynamic analysis of calcite twins (Turner and Weiss, 1963).

Paleostresses determined on the basis of fault-slip data

The inversion method

The stress inversion method is based on the following assumptions: (a) Slip along a fault occurs in the direction of maximum resolved shear stress. (b) The shear and normal stresses on the fault satisfy the Coulomb-Mohr yield criterion $\tau > C + \mu\sigma_n$, where τ and σ_n are the magnitudes of the shear and normal stresses in the slip direction, C is cohesion and μ is the coefficient of friction.

(c) The slip event occurred under relatively uniform stress conditions.

The calculated stress tensor for each fault population is the least-squares solution for the complete group of faults, with some misfit of the individual faults (Reches, 1987b). The tensor of the complete group is called the general tensor. The mean misfit angle between the principal stress axes of the general tensor, and the stress axes of the ideal tensors associated with the individual faults is called the principal axes misfit angle (PAMA). An ideal stress tensor of a fault requires the least shear stress to maintain slip along that fault. A second type of misfit is the slip misfit (SM), which is the angle between the axis of the maximum resolved shear stress on the fault plane, and the slip observed in the field.

The general stress tensor and the misfit angles are determined for the original group of faults measured in the field. A fault is deleted from this group if the principal axis misfit is large (typically larger than 60°), or if the slip misfit is larger than 90°. In this procedure, the original group is separated into a primary and a secondary set; the faults of the primary set fit the general solution, whereas the faults of the secondary set do not. A stress tensor is also calculated for the secondary set, and in some cases it provides a sound solution which differs from the solution of the primary set. In other cases, there is either a small number of faults in the secondary set, or these faults do not fit any systematic solution and they are rejected as "noise". This procedure for separation of tectonic phases is applicable when the faults of one phase are more abundant in the original group. If the faults of the two phases are of equal abundance, the separation into two sets is based on structural considerations mentioned below.

Fault slip data in Ramon domes

We computed the stress tensors for 326 faults in five stations in the Gevanim Dome, four stations in the Saharonim Dome, one station in the Afor anticline, between the domes and two stations in the Neqarot structure (Neqarot and Parsa), south of the Saharonim Dome, in the downthrown block of the Ramon fault (locations in Fig. 1).

Faults in Gevanim, Saharonim and Afor were measured in the same stratigraphic unit—limestones of the Triassic Saharonim Formation; faults in the Neqarot area were measured in limestones of the Late Cretaceous. The fault stations in Gevanim and Saharonim are located at similar structural positions: within the steeply dipping layers at the limbs of the domes (Figs. 1 and 3).

The measured faults vary in length from 1 m to a few hundred meters, and displacements range from several centimeters to tens of meters. The inclination of the fault plane, the slip axis and the sense of slip were measured for each fault. Stations vary in size from a few tens of square meters in a single outcrop to a few hundred meters long and a few tens of meters wide.

Analysis of the faults

The faults measured in seven stations: Gevanim-South, Gevanim-West, Saharonim-Northeast, Saharonim-Southeast, Neqarot, Parsa and Afor, yielded a single stress tensor; small misfit angles were obtained for almost all faults of each station. Only few faults with large misfit angles had to be deleted (Table 1).

In the Gevanim-East station the original group of 40 faults was separated according to the misfit angles into two subgroups of 22 and 12 faults each. Both these groups yielded sound solutions with small misfit angles; the 6 remaining faults, which did not fit any solution were deleted.

In two stations, Gevanim-North and Saharonim-North, the solution for the complete groups of 40 and 61 faults, respectively, yielded large misfit angles (PAMA = 52.6° and 30.5°; SM = 44.5° and 44.8°). By rejecting the faults with large misfit angles, we obtained primary subgroups of 30 and 49 faults respectively, which yielded sound stress solutions (Table 1). The two secondary subgroups of 10 and 12 faults, did not yield sound solutions and were rejected as noise.

In the Gevanim-Northwest station the solution for the entire group of 30 faults has high misfit angles (PAMA = 49.3°; SM = 22.6°), as this station probably includes two fault populations of approximately equal abundance. Thus, the separation procedure according to the misfit angles is

TABLE 1

Fault stations and results of the stress analysis

Stations and substations	Number of faults [a]		Calculated stresses				Average bedding dip (°)	Estimated friction [c]	PAMA [d] (°)
			trends		magnitudes [b]				
	acc.	rej.	σ_1 (°)	σ_3 (°)	σ_1	σ_3			
Gevanim Dome									
West	16	2	63/216	26/ 21	1.01	0.99	12	0.0	14
North West I	18	3	7/115	3/ 24	1.29	0.45	20	0.5	14
North West II	9		79/267	6/ 31	1.03	0.18	20	0.8	20
North	30	10	81/137	7/289	1.02	0.13	50	0.8	42
East I	22	6	72/ 28	5/135	1.09	0.12	27	1.0	27
East II	12		40/221	49/ 48	1.02	0.99	27	0.0	20
South	14	6	4/127	0/ 37	1.13	0.87	40	0.1	21
Saharonim Dome									
West	22	2	23/150	1/240	1.42	0.46	35	0.5	22
North	49	12	25/146	0/ 55	1.01	0.98	40	0.0	24
North East	13	1	16/161	3/252	1.64	0.52	25	0.5	17
South East	16	1	0/335	4/245	1.50	0.60	24	0.4	17
Stations away from domes									
Afor	14		11/312	2/ 42	1.73	0.62	15	0.5	11
Parsa	32		4/136	0/226	1.28	0.20	20	0.9	13
Neqarot	16		7/116	1/206	1.39	0.68	0	0.3	20

[a] acc.—accepted faults of the group; rej.—rejected faults of the group.
[b] As a fraction of the vertical, lithostatic stress.
[c] Estimates of friction coefficients according to the principal axes misfit.
[d] Principal axes misfit.

not applicable in this case, and the original faults were separated according to the sense of slip: a primary group of 18 strike-slip faults and a secondary group of 9 normal faults (Table 1); 3 faults, which did not fit any solution were deleted.

The solutions with the smallest principal axes misfit angle, PAMA, were selected for each station or subgroup. The selected stress tensors are plotted on stereonets (Fig. 5), presented as stress trajectory maps (Fig. 6) and summarized in Table 1.

Results: the calculated paleostress tensors

Gevanim Dome. Two different states of stress were computed for fault groups in the Gevanim Dome (Figs. 5a, 6). The first state of stress includes a subvertical maximum compressive stress, σ_1, and the intermediate and the least compressive stresses oriented in radial and tangential directions with respect to the dome (Fig. 6a). The magnitudes of σ_2 and σ_3 are almost equal. This stress state was found in four stations: Gevanim-East, North, West and in the secondary group of Gevanim-Northwest (Fig. 5a).

The second state of stress includes subhorizontal σ_1, trending N55°–65°W, subhorizontal σ_3 trending N25°–35°E and vertical σ_2 (Figs. 5a, 6b). This stress state was found in the Gevanim-South and in the Gevanim-Northwest stations (Figs. 5a). In the two groups of the Gevanim-East station the directions of the principal stress axes are similar but their relative magnitudes are interchanged. This similarity suggests that the two groups were not formed under a completely different state of stress, but rather, indicate variations of a single state of stress (see Jackson, 1987).

Saharonim Dome. The principal stress axes σ_1 and σ_3, are subhorizontal in all stations of the Saharonim dome (Figs. 5b, 6c). The maximum

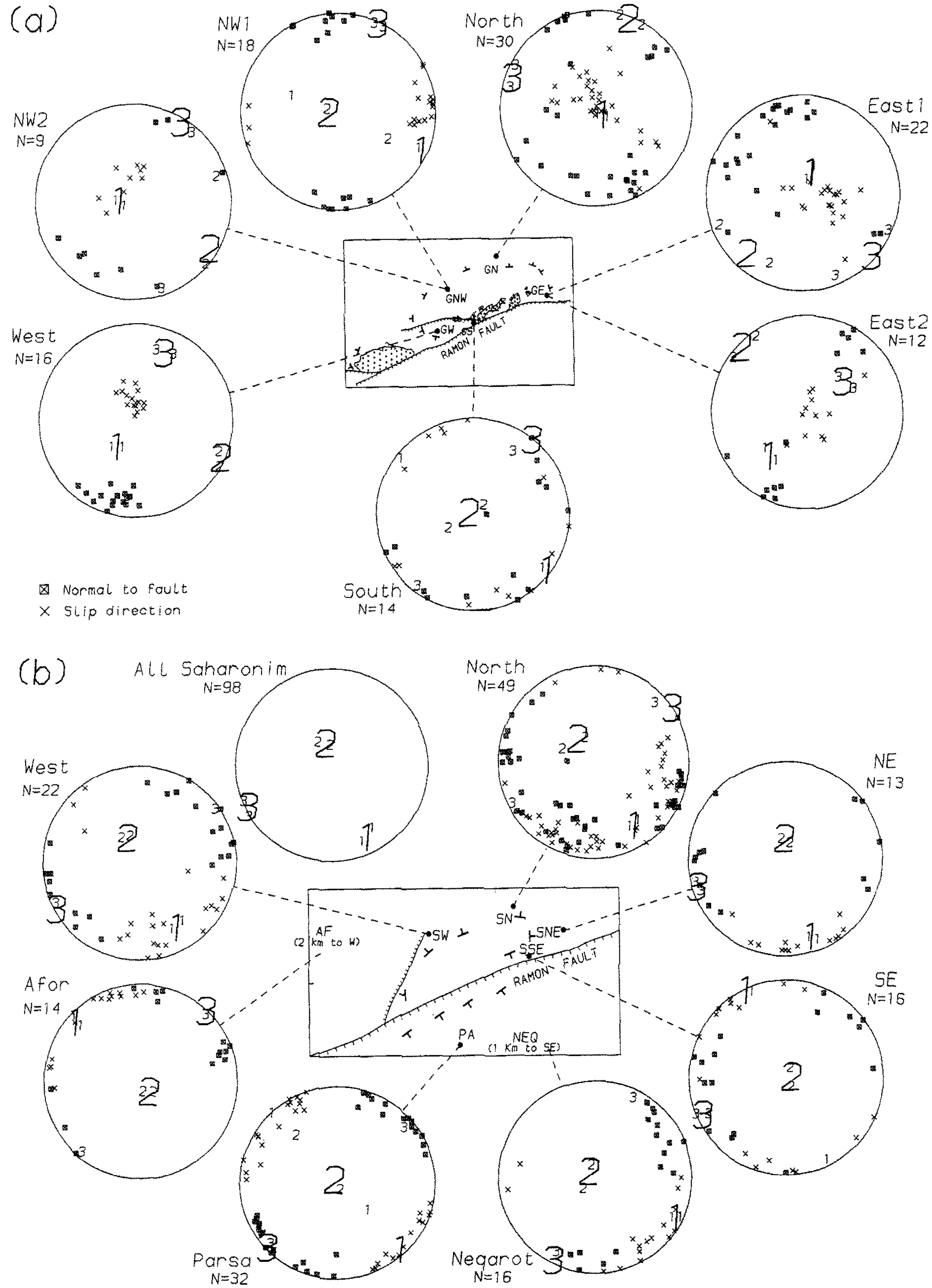

Fig. 5. Stereographic projections of the computed stress tensors in Ramon domes and surrounding areas according to stress inversion of fault slip data (see text). Bold numbers show the principal stress axes for the least mean squares solution, and small numbers mark the solutions for first and second standard deviation levels. (a) Gevanim Dome. (b) Saharonim Dome and adjacent stations.

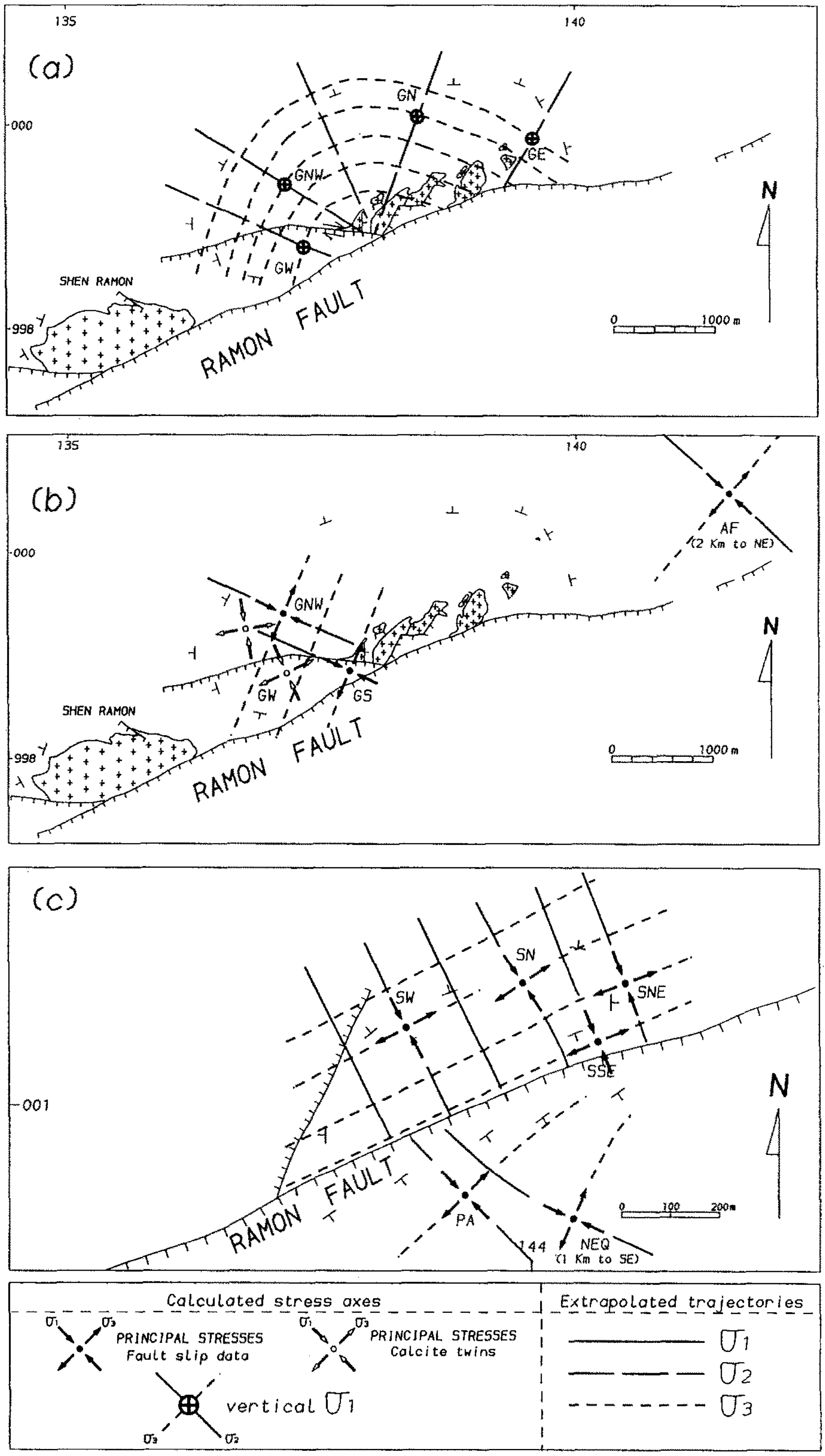

Fig. 6. Tectonic stress trajectories in the Ramon domes. Legend of structural elements in Fig. 1. a. Gevanim Dome, intrusive stage. b. Gevanim Dome, horizontal compression stage. The stress axes determined from calcite deformation twins are marked in their location. c. Saharonim Dome.

compression axis σ_1 trends N20°–35°W and the least compressive axis trends N55°–70°E. The relative magnitude of each of the three principal stress axes is different.

Afor and Negarot structures. Faults were measured in these structures, away from the domes, to obtain the regional state of stress. The stress tensors calculated for Afor and Parsa are similar to each

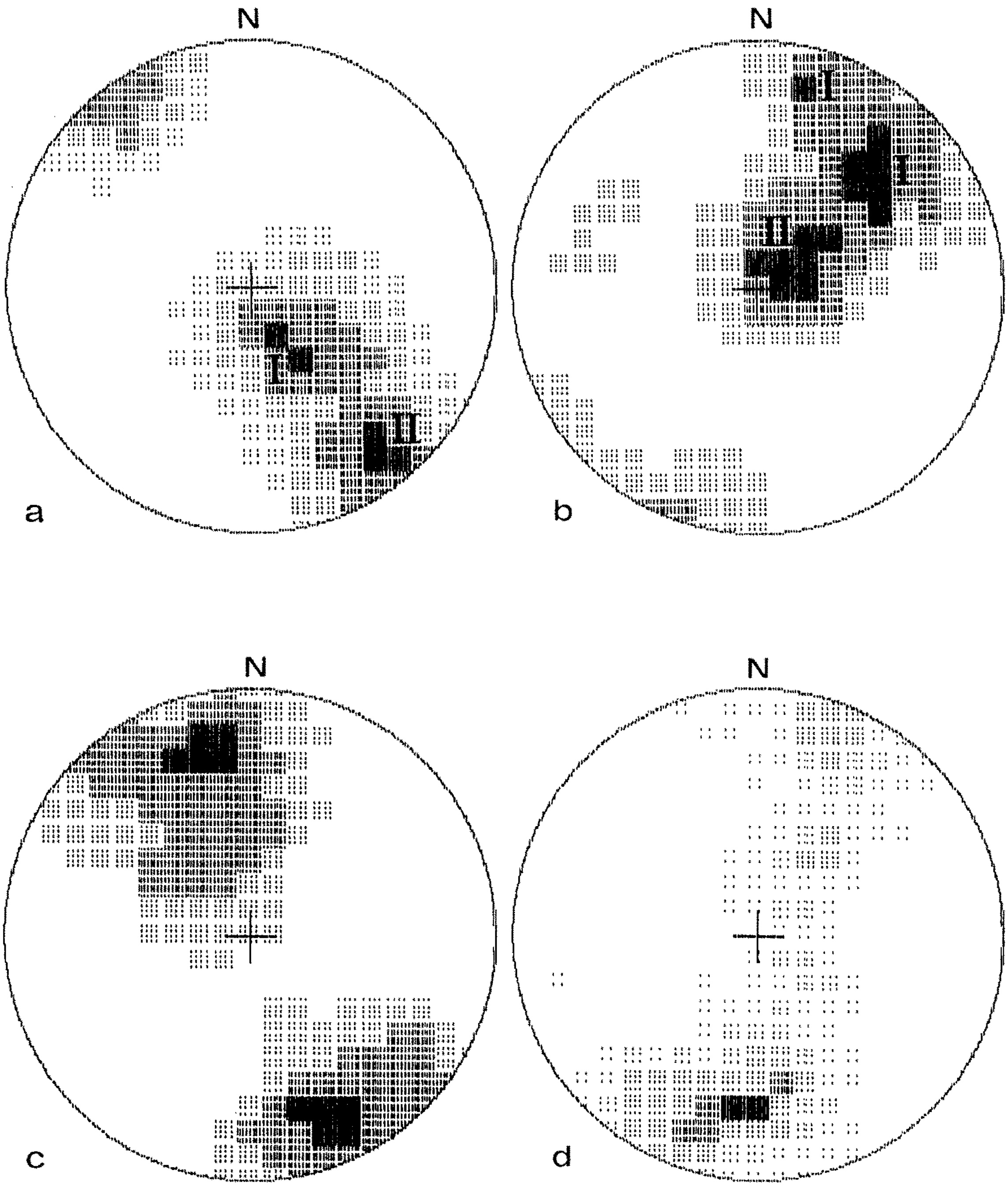

Fig. 7. Stereographic projection of the stress axes determined from calcite deformation twins in Gevanim Dome. Lower hemisphere, equal area projection; contouring following Kamb's method; contour intervals are at: expected density, 2, 4, and 6 standard deviations above expected. (a) Maximum compression and (b) minimum compression in sample GR-260, collected in station GW (Fig. 1b); results of 77 grains. (c) Maximum compression and (d) minimum compression in sample GR-237, collected in station GNW (Fig. 1b); results of 58 grains. Numbers *I* and *II* indicate the two possible deformational stages (see text).

other (Figs. 5b, 6b, 6c): subhorizontal σ_1, trending N45° W and subhorizontal σ_3 trending N45° E. In Neqarot the stresses are rotated by 20°: σ_1 is subhorizontal trending N65° W and σ_3 is subhorizontal trending N25° E.

Paleostress determined from calcite twinning

Principal stress axes were determined from calcite deformation lamellae at two locations in the Gevanim Dome by using the dynamic method of Turner and Weiss (1963). One sample, GR-260, is from a zone of calcite mineralization along a N70° W trending dike in the Gevanim-West station. The other sample, GR-237, is from calcite veins on a strike-slip fault trending N85° W, in Gevanim-Northwest. The paleostress axes which have been determined from these two samples show slight variations (Fig. 7). The σ_1 axes range between subvertical and subhorizontal in the general trend of N20°–30° W. The σ_3 axes are more scattered; they form one subvertical and a few subhorizontal clusters trending N5°–45° E.

This distribution of the calcite stress axes could not develop under a simple state of stress. For the sake of simplicity, we assume that the twinning developed under two separable states of stress (a similar distribution would develop during the transition period between these two states). The first stress state (*I* in Fig. 7a and 7b), includes subvertical σ_1 and subhorizontal σ_3 trending N5°–45° E. The second stress state (*II* in Fig. 7a, b), includes subhorizontal σ_1 trending N30° W, and subvertical σ_3.

As both calcite samples show evidence for a maximum compressive stress trending subhorizontally in N20°–30° W direction and as one sample also indicates subvertical σ_1 (Fig. 7a), we conclude that the the calcite stress directions are in general agreement with the stress directions calculated by the stress inversion method (Fig. 5).

Summary: paleostresses in the Ramon domes

Paleostress tensors computed for the fault populations and the analysis of calcite twinning, yielded the following paleostresses for the Ramon domes and the adjacent structures (Figs. 5–7):

(a) Subhorizontal σ_1 in N20°–35° W direction which dominates the Saharonim Dome and calcite twinning stations in the Gevanim Dome.

(b) Subhorizontal σ_1 in N45°–65° W direction which is found in two stations in the Gevanim Dome and in the three stations outside the domes.

(c) Subvertical σ_1 which is found only within the Gevanim Dome.

It follows that a uniform state of stress with subhorizontal compression prevailed in all stations of the Saharonim Dome, and slightly rotated stresses prevailed in the surrounding areas. In the Gevanim Dome, an additional stress with subvertical compression prevailed.

All the faults stations in both domes are located within a similar stratigraphic unit and in a similar structural position (see above). Therefore, the different states of stress within and between the domes reflect, in our opinion, different deformation history, rather than variations in the stress due to structural position or height within the bending sequence (e.g., Withjack and Scheiner, 1982, Jackson, 1987).

Deformation of sedimentary layers by a rising intrusion: a model for the Gevanim Dome

The Gilbert model

The initial stage of doming at Gevanim is related to the emplacement of a central igneous intrusion; this observation is justified below by a model for doming above an igneous intrusion. First however, we summarize the main observations so far:

(a) The central quartz-syenite intrusion has an elliptical geometry in map view and a box shape in cross sections (Figs. 2, 3); the roof of the intrusion is composed of subhorizontal, concordant sectors, connected by short, vertical segments of piercement faults (Fig. 3a).

(b) Excluding a few piercement faults along the contacts of the central intrusion, most faults in the sedimentary layers are concentrated within a belt along the eastern, northern and western flanks of the dome (Fig. 1b). Faults suitable for the stress inversion analysis (faults with measured slip axis and sense), were found primarily in this belt.

(c) the subsurface extension of the intrusion, as deduced from the TDEM survey coincides with the outline of the Gevanim Dome (Fig. 2).

(d) Two states of tectonic stresses were determined. One has vertical maximum compression and radial and concentric distribution of the intermediate and least compressive stresses (Figs. 5a, 6a). The second stress state has subhorizontal compression trending N70° W and N20° W (Figs. 5a, 6b, 7).

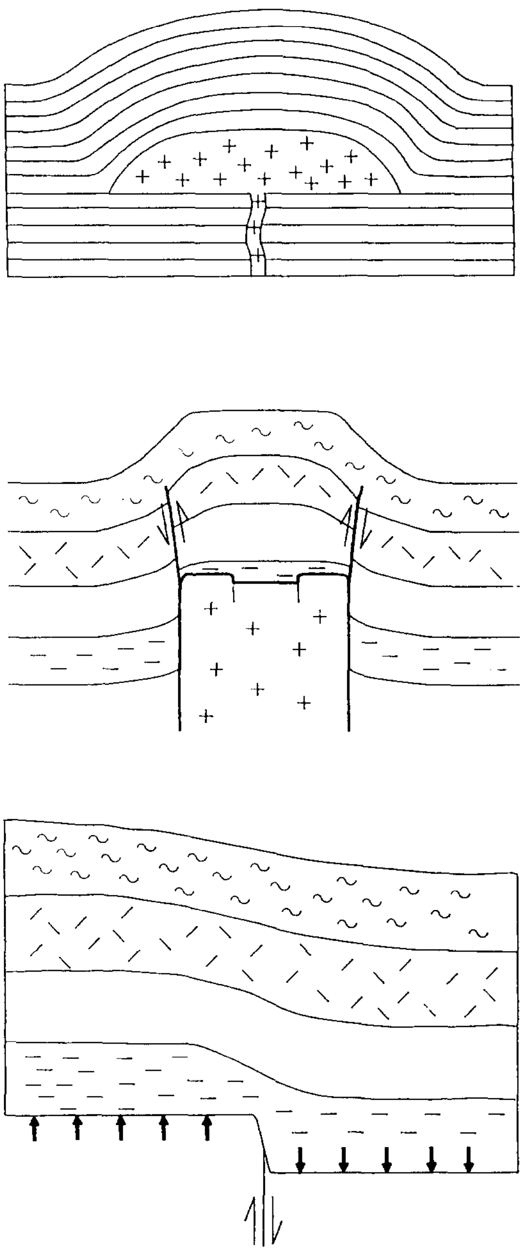

(a) (b) (c)

Fig. 8. Idealized models for the emplacement of the Gevanim intrusion. a. Gilbert's model for laccolithic intrusions. b. A generalized geometry of the stepped intrusion in Gevanim. c. The drape folding model of overburden deformation above a vertical fault (after Reches and Johnson, 1978).

The relations between the intrusion and the host rocks in the Gevanim Dome resemble the classical laccolith model of Gilbert (1877) (Fig. 8a). He suggested that laccoliths initiate when magma spreads as a sill between two sedimentary layers. When the sill attains a critical diameter, the pressure of the magma is sufficient to break and bend the overburden layers along the circumference of the intrusion. Once the circumference yields, the laccolith inflates, to form a mushroom-shaped intrusion with flat, concordant roof, bound by a circumferential zone of faulting and bending. In Gilbert's idealized model the intrusion is envisioned as a rising piston bound by a cylindrical peripheral fault (Johnson, 1970, ch. 2). Pollard (1968), Johnson (1970) and Jackson and Pollard (1988) explored and expanded Gilbert's model.

According to our observations in the Gevanim Dome, the model of Gilbert is the most applicable one: The roof of the intrusion is flat and concordant, piercement faults have been mapped in the center of the dome and a 2 km long concentric peripheral fault encircles the north and east limbs of the dome (Fig. 1b). The maximum vertical displacement along this concentric fault is around 50 m, whereas the total uplift by the intrusion at the center of the dome is at least 100 m (see above). Thus, the total uplift in Gevanim is attained by both flexing of the overlying strata and step-wise displacements along peripheral and piercement faults (Fig. 3a, 8b).

The analytical solution

Any analysis for the three-dimensional deformation of a dome by both bending and faulting is complicated. Thus, we present an analysis which is restricted to bending in a dome under plane strain conditions. We utilize the solution for drape folding of Reches and Johnson (1978), by which one can derive the deformation of a two-dimensional stratified sequence in response to vertical faulting in the underlying substratum (Fig. 8c). This configuration is similar to the Gevanim Dome. The step-like displacement caused by the rising Gevanim intrusion and the peripheral faults resemble the displacement along a vertical fault in the substratum of the drape folding model; the bending of the strata in Gevanim resemble the draping of the overlying layers in the drape folding model (Fig. 8c). The stress analysis and the derivation of the basic equations are outlined in the Appendix and described in detail by Reches and Johnson, (1978, appendices I and II).

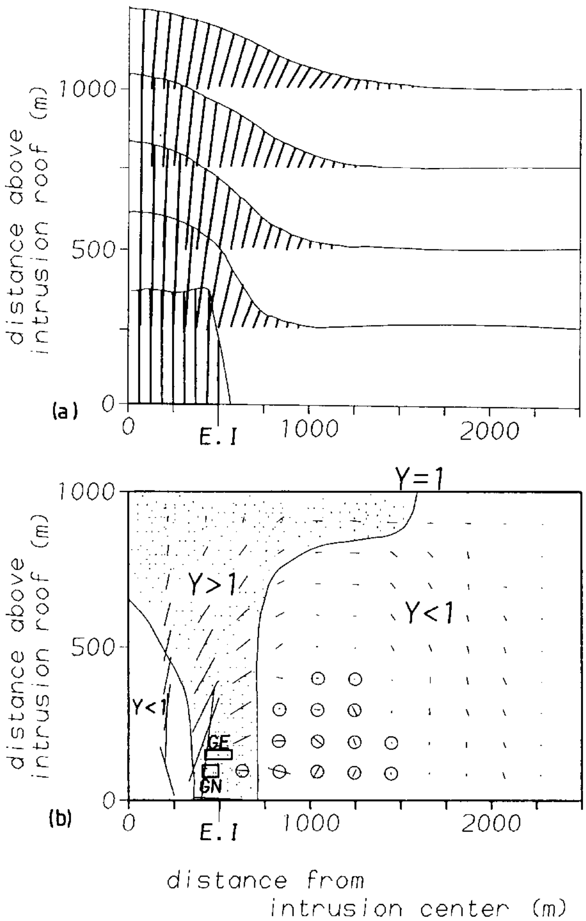

Fig. 9. Displacements and stresses in a drape fold model of 1 km thick incompressible elastic plate, deformed by a 1 km wide intrusion at the base (see Appendix). Young modulus is 50 GPa; the model is two-dimensional, and only the right half is shown due to its symmetry. *E.I.* marks the edge of the intrusion. a. The displacement field associated with 0.5 m uplift at the base. Displacement magnitudes are exaggerated by 10^3. b. Orientations of the maximum compressive axes associated with the displacement field of (a). The model is divided into regions according to yielding index Y, where $Y=(\sigma_1-\sigma_3)/(1.7\sigma_{\text{vertical}})$ (see Appendix). Yielding occurs for $Y>1$. Gevanim-North station (GN) and Gevanim-East station (GE) are marked in their approximate location.

The two-dimensional model of uplift of the sedimentary rocks is symmetric with respect to the center of the intrusion, thus, displacements and stress fields are shown only for one flank (Fig. 9). The thickness of the deformed plate in the model is 1000 m, and the width of the intrusion is 1000 m (Fig. 9); these dimensions are approximately the field dimensions. The vertical displacement (uplift) used in the calculation is small, 0.5 to 1 m, to maintain the linearity of the elastic solution (see Reches and Johnson, 1978). The inferred location of the field stations Gevanim-North and Gevanim-East is approximately 100 m above the intrusion and close to the peripheral fault (Fig. 9b).

Model predictions

The deformation of a 1000 m thick layer due to 1 m uplift by a 1000 m wide intrusion is shown in Fig. 9. The figure shows the distribution of the displacement at four levels in the plate (Fig. 9a), the orientations of the maximum compressive stress axes and the zones in which the Byerlee yield condition is exceeded (Fig. 9b; see also the Appendix) at the initial stage of deformation.

The base of the plate which directly overlies the top of the intrusion is displaced vertically, and the base of the plate away from the intrusion is not displaced; a narrow transition zone appears between the two regions (Fig. 9a). The transition zone becomes wider upward in the plate, and it includes both vertical and horizontal displacements.

The orientations of the maximum compressive stress vary in both the vertical and horizontal directions. The most profound change in stress orientations occurs close to the margins of the intrusion in the transition zone, where the maximum compression rotates from vertical above the intrusion to almost horizontal a few tens of meters away from the intrusion (Fig. 9b). The zone in which yielding conditions for faulting are exceeded is restricted to the transition zone at depth and it widens upward (Fig. 9b). A particularly significant result is that the stresses directly above the intrusion are below the yielding conditions; thus, one anticipates less faulting in this region.

Application to field observations

The model derivations bound the field observations and the stress tensors. The model predicts that stations with subvertical σ_1 should be located directly above the intrusion or in the transition zone. Further, the model predicts that faulting is more abundant in regions with stresses which exceed the faulting yield condition; this yield condition is not satisfied directly above the intrusion (Fig. 9b), but rather within the transition zone. Therefore, according to the model, a station with both subvertical σ_1 and evident faulting should be restricted to a portion of the transition zone during the initiation of the uplift.

This deduced location is in agreement with the field observations. The stations with subvertical σ_1 axis, Gevanim-East, North, and Northwest, are distributed along the margins of the dome (Figs. 1b, 5a). The exact location of Gevanim-North station with respect to the intrusion is known from the TDEM survey (Fig. 2): the margin of the intrusion is about 100 m north of the station and the top of the intrusion is approximately 100 m below the station (section 2 in Fig. 3a). This location is projected as area *GN* in the theoretical model (Fig. 9b), and is well within the portion of the transition zone where faulting is predicted by the model (lower rectangle in Fig. 9b).

In the Gevanim-East station, two states of stress were computed: one with vertical σ_1 and the other with subhorizontal σ_1. The model predicts rapid changes from vertical to horizontal σ_1 above the termination of the intrusion, and indeed, the Gevanim-East station is located both above and away from the edge of the intrusion (upper rectangle in Fig. 9b). Thus, the two stress tensors calculated for Gevanim-East, may reflect spatial variations within a single state of stress, rather than two separate tectonic phases.

One striking feature in the Gevanim Dome is the distribution of faults. Most faults occur within a belt around the dome (Fig. 1b); this belt includes all Gevanim stations and the 2 km long concentric fault regarded above as the upward continuation of the intrusion's peripheral fault. The formation of such fault belt suggests that the stresses within the belt were larger then elsewhere. The location of the fault belt overlaps the subsurface margin of the intrusion (Figs. 2, 3a), and corresponds to the transition zone with its high yielding index in the model (Fig. 9b). The few faults mapped in the central part of the dome have small displacements, moreover they are restricted to the vertical contacts of the intrusion, and are regarded as piercement faults. They are not located within the transition zone. The unfaulted zone which separates the center of the dome from the peripheral faults corresponds to an area with low yielding index in the model.

In summary, the present model for bending above an intrusion explains the orientations of the maximum compressive stresses in Gevanim fault stations, the location of the faulting belt around the dome, and the lack of major faulting in other parts of the Gevanim Dome.

Discussion: the structural development of the Ramon domes

Folding–faulting temporal relationship

The accurate determination of the paleostress tensors in the inclined layers of the domes, provides a tool to resolve the temporal relations between faulting events and the doming processes. The inclination of the layers increases with the progress of the doming, thus, under constant state of stress, faults which developed during early stages of the doming, would have different orientation than faults which developed later.

At this point we make two assumptions: First, the principal axes of the tectonic stresses were horizontal and vertical during the period of their activity. This is a simplifying assumption which is commonly used in stress analyses (e.g., Oppenheimer et al., 1988). Second, faults change their attitudes as the host layer increases its inclination without changing the fault-layer geometry. Thus, ancient faults passively rotate during doming. By comparing the stress tensors obtained for the present position of the layers (fully inclined), with the stress tensors obtained for the retilted layers (to the horizontal), one gets the relative age of the faulting with respect to doming. For example, the σ_1 axes of the various stations do not converge into one axis by the rotation of the host layers to horizontal position (Fig. 10). This observation of non-converging σ_1 axes indicates that the flanks of the domes did not develop simultaneously, and further, that faulting and folding were not contemporaneous.

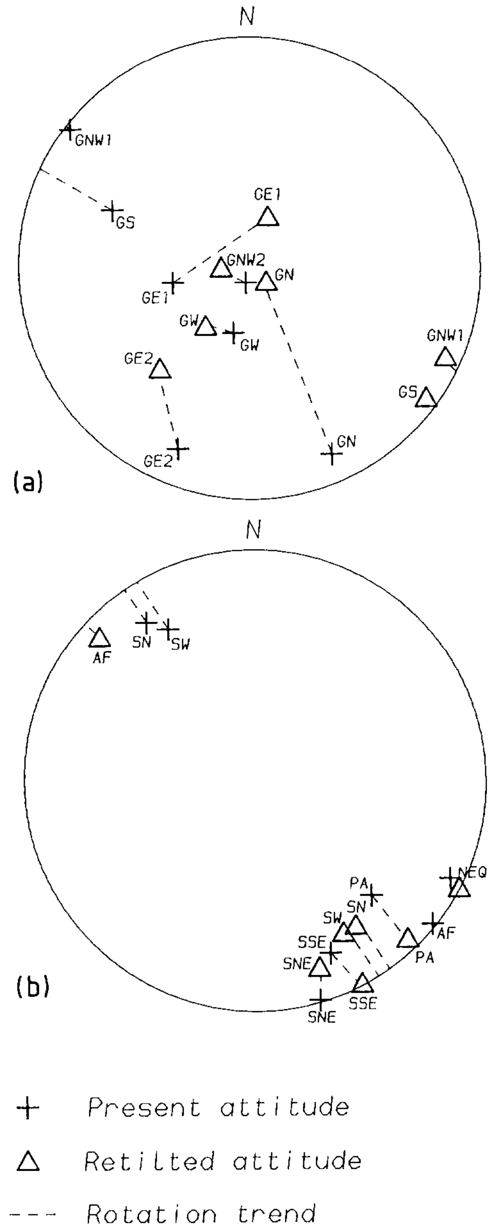

Fig. 10. Stereographic projection of maximum compressive stresses of all Ramon stations at present layer attitudes and retilted attitudes. a. Gevanim Dome. b. Saharonim Dome and adjacent stations.

Gevanim Dome

The two tectonic stress tensors in Gevanim dome, one with a vertical σ_1 and the other with a horizontal σ_1 (Figs. 5a, 6a, b) indicate two deformation phases. It appears that the phase with vertical σ_1 predated the tilting of the layers of the dome, because the steep σ_1 axes of this group are better clustered around the vertical axis in the retilted position (Fig. 10a). The σ_1 axes of the second tectonic phase, are subparallel to bedding in the southern limb, where the layers dip 30°–40° (Fig. 10a), thus suggesting that the second faulting phase also predated the folding of the southern limb. In the northwest limb, where the layers dip 10°–15°, folding-faulting temporal relationship of the second faulting phase cannot be resolved due to the relatively low sensitivity of the method.

Saharonim Dome

The σ_1 axis is parallel to bedding in the southeast limb (Fig. 10b), thus indicating that the faulting predated the folding (tilting) of this limb. On the other hand, σ_1 is horizontal in the present attitude of the northeastern limb, suggesting that there, the folding (tilting) predated the faulting. In the northern and western limbs σ_1 axes are inclined in both attitudes, but become horizontal for partial retilting of the host rocks; this suggests that either faulting occurred between two or more folding phases or that faulting and folding occurred penecontemporaneously.

The folding-faulting relations deduced for the Saharonim Dome are consistent with the Triassic angular unconformity first described by Zak (1957). He showed that during the Middle-Triassic a block tilted by as much as 24° to the north, existed north and northeast of the Saharonim Dome (Fig. 3b, section 5). This Triassic tilting predated the faulting stage which we measured, thus, the faulting in the northern part of the dome occurred while the host layers were partly tilted. The major doming phase in Saharonim which folded both the southern and the northern flanks of the dome took place after faulting terminated.

Relations of the Ramon domes and the Ramon fault

The Ramon fault zone is part of the 250 km long, Sinai–Negev right-lateral shear zone. The Ramon zone has been active since the Triassic (Garfunkel, 1964), but the faulting mode of its early activity is not clear. Lateral motion became evident only since the Early Miocene. 2.5 km of right-lateral slip was documented along the Ramon Fault zone, in the Minshera region, about 120 km west of the present study area (Bartov, 1974). The magnitude of right-lateral slip in the Ramon area is unknown, but it is assumed to be less than 2.5 km (Garfunkel, 1964).

Many domes are associated with the strike-slip faults of the Sinai–Negev shear zone (Bartov, 1974) and elsewhere (e.g., Aydin and Nur, 1982); however, the Ramon domes reveal no simple relationship to the Ramon fault. In contrast to the post-Early Miocene lateral slip along the fault, doming at Gevanim initiated during the Early Cretaceous emplacement of the central intrusion, and the folding at Saharonim initiated during the Triassic tilting of Saharonim region. Thus, the initiation of the Ramon domes is not related to the strike-slip motion of the Ramon fault. The structural and temporal relations between the fault and the domes are restricted to the late stages of doming during the Late Cretaceous to Recent time. During this period the Saharonim Dome was subjected to horizontal compression in N20°–35°W direction and the Gevanim Dome was subjected to subhorizontal compression, in N55°–65°W and in N20°–30°W direction. These trends of the stress axes are slightly different than the regional stress field of the "Syrian Arc" and "Dead Sea", defined by Eyal and Reches (1983). Therefore, the two states of stress determined for Ramon domes are not necessarily correlated with the two regional stress fields. Further, the stress states in Ramon seem to be contemporaneous, whereas the regional fields prevailed at separated periods and were restricted to different areas (Eyal and Reches, 1983).

The variations in the stresses which we observed along the Ramon fault are better perceived in the light of recent studies of the state of stress along the San Andreas fault in central California (Zoback et al., 1987). These authors found that σ_1 axes within a region of up to 100 km width on both sides of the San Andreas fault are roughly perpendicular to the fault. However, right-lateral slip along the San Andreas fault requires an angle of 30°–45° between the maximum compressive stress axis and the fault. Zoback et al. (1987) explained this discrepancy between the observed and the expected stress orientations by the weakness of the San Andreas fault, which may cause rotation of the tectonic stress field at the proximity of the fault. Indeed, in California, the far-field principal stresses have maximum compression at an angle of 50° to 55° to the San Andreas (Zoback et al., 1987). It is possible to interpret the stress configuration in Ramon in a similar manner to the interpretation of the stress field in California presented by Zoback et al. (1987). According to this interpretation, the regional, remote stress during post-Turonian times, was the Syrian Arc stress field as defined by Eyal and Reches (1983); the maximum compression of this field was subhorizontal in N70°W direction. The compression axes of N20°–30°W and N45°–65°W, determined for the Ramon domes (Fig. 5), are then local stresses, rotated at the proximity of the Ramon fault. If such stress rotation occurred along the Ramon fault, then the Ramon domes were amplified by fault-normal rotated compression, similarly to the folding processes in central California, as suggested by Zoback et al. (1987).

Structural development of the Ramon domes

In the light of the calculated stress tensors, the field relations between the intrusions and the domes, and previous studies of the Ramon fault zone and the regional stress fields, we propose the following structural history of the Ramon domes since the Triassic (Fig. 11):

Middle–Late Triassic

The area of Saharonim dome was tilted northwards with a structural high close to the present dome; the angular unconformity reaches 24° on the flanks of the structure. This tilting developed due to normal faulting either along the Ramon fault (Zak, 1963; Freund et al., 1975) or along

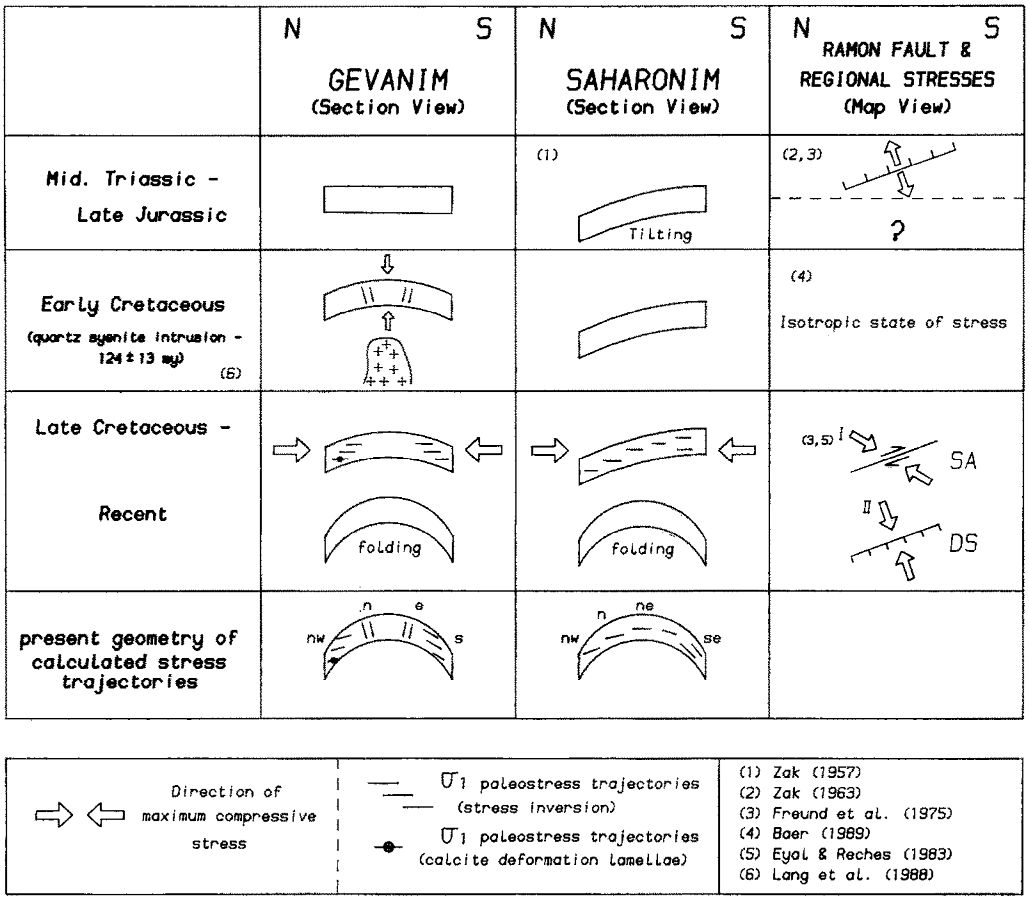

Fig. 11. Structural development of the Ramon domes according to the present stress analysis. The geometry of the domes is shown schematically; the maximum compressive axes of the paleostresses are displayed as thin lines shown first at the time of their assumed activity, and then rotating rigidly with the layers. Regional stresses proposed in previous investigations are shown in the right column.

other faults which bound a regional basin (Garfunkel and Derin, 1985). Some differential subsidence was also described north of Gevanim (Garfunkel, 1964), but the exact geometry of this structure is unknown. The Middle to Late Triassic tectonic phase left no paleostress indications in form of faults or calcite twinning.

Late Triassic–Late Jurassic

The southern Ramon area was uplifted at the end of the Triassic (Zak, 1963); during the Early Jurassic the area of Ramon was subjected to intense differential movements and during the rest of the Jurassic local movements ceased and regional subsidence commenced (Garfunkel and Derin, 1984). No evidence was found for the development of the Ramon domes during this period.

Late Jurassic–Early Cretaceous

Intrusive magmatism and regional uplift dominated the tectonic activity in southern Israel. A conspicuous radial dike system with individual dikes up to 20 km long, dominates the Ramon sheet intrusions (Zak, 1957). A stress analysis of this system indicates a lithostatic (Anderson's isotropic) state of stress (Baer, 1989). The first doming stage of Gevanim is the uplift, bending and faulting of the sedimentary strata, in response to the intrusion of a quartz-syenite stock 124 Ma ago (Lang et al., 1988). The maximum compressive stress in the limbs of Gevanim dome was vertical and the intermediate and minimal stresses were radial and concentric with respect to the dome symmetry (Fig. 6a). No deformation has been recognized in the Saharonim Dome or along the Ramon fault during this period.

Late Cretaceous–Recent

The regional, remote stress field in the Ramon area is regarded as the Syrian Arc stress, with maximum compressive axis trending N70° W (Eyal and Reches, 1983). This remote stress is rotated at the proximity of the Ramon fault into the compressive axes of N20°–65° W determined in the domes and their adjacent areas. During this period the two domes were amplified under layer-parallel compression directed approximately perpendicular to the Ramon fault.

Summary

We analyzed the doming mechanisms of two domes developed along the Ramon fault, southern Israel. Even though the domes are in the same tectonic environment and have similar aspect ratio, they originated by distinctly different mechanisms. The Gevanim Dome developed under layer-perpendicular compression associated with the emplacement of a large quartz-syenite intrusion. The state of stress during the intrusive stage was with a vertical σ_1, a radial σ_2 and a circumferential σ_3. The intrusion geometry, domal bending and the state of stress in Gevanim Dome are successfully simulated by a two-dimensional analytical model of drape folding. We demonstrate that the subsurface structure of the igneous body may be estimated from paleostress measurements in the overlying sedimentary rocks. The Saharonim dome, on the other hand, lacks a major intrusion, and it initiated as a tilted block.

The initial structures, namely, a dome above an intrusion in Gevanim and a tilted block in Saharonim, were amplified since the Late Cretaceous. During this stage both domes were subjected to horizontal compression with σ_1 trending N20°–65° W. Even though these stress directions roughly correlate with regional stress fields determined by Eyal and Reches (1983), it is possible that the calculated stress fields reflect rotated stresses at the proximity of a weak Ramon fault.

Acknowledgments

We wish to thank Marie Jackson for the critical review and discussions which significantly improved this paper. The discussion with Zvi Garfunkel and Joseph Bartov are greatly appreciated. Thanks to Saadya Levy for his technical assistance, and to Yossef Levy for the photographic work. Yossi Mart and an anonymous reviewer made many helpful remarks.

The study is part of a Ph.D. dissertation of the senior author in the Hebrew University, Jerusalem, and it was supported by project 20024 of the Israel Geological Survey, Jerusalem.

Appendix

Application of the drape folding model to the laccolith model

Drape folding is one mode of monoclinal flexuring (Reches and Johnson, 1978). The drape folding model includes a multilayer with a free upper surface, deformed over a faulted substratum (Fig. 8c). Below we solve the case for a single thick layer when the underlying substratum is subjected to vertical displacement. The solution is for incompressible linear elastic plate under plane strain conditions.

The basic equations present the stresses, displacements and strains associated with a single sinusoidal wavelength of a single layer (eqns. 21, appendix 2 in Reches and Johnson, 1978). To simulate a step-like displacement above the vertical fault at the base of the plate, one may use a Fourier series which is the sum of many wavelengths (eqns. 22–25 and fig. 14 in Reches and Johnson, 1978). We use the series:

$$V = \frac{2}{L} \sum_n \sin\frac{n\pi}{2} \cdot \frac{\sin(0.1n\pi)}{0.1n\pi} \sin\frac{n\pi x}{L}$$

where $L = 500$ m and x is the distance from the center of the intrusion. The calculations include solutions of the displacements, stresses and strains for up to 120 wavelengths ($n = 120$), and summation of the individual waves to obtain the complete deformation (see also Reches and Johnson, 1978).

To locate the regions of likely yielding within the model, a yielding condition was calculated for each point in the model. Brace and Kohlstedt (1980) showed the strength of crustal rocks at shallow depth is $(\sigma_1 - \sigma_3) > 1.7\,\sigma_n$. We made the approximation that $\sigma_{\text{vertical}} \approx \sigma_n$, where the vertical stress is:

$$\sigma_{\text{vertical}} = -Rgz$$

where R is the mean rock density, g is the earth's acceleration and z is the depth. When the principal stresses calculated by the model, and the vertical stress satisfy the last equation at a given point of the model, then this point is regarded to be at a yielding stage.

References

Aydin, A. and Nur, A., 1982. Evolution of pull-apart basins and their scale independence. Tectonics, 1: 91–105.

Baer, G., 1989. Igneous intrusions in Makhtesh Ramon, Israel: Mechanics of emplacement and structural implications. Ph.D. Diss., Hebrew Univ., Jerusalem, 93 pp. (in Hebrew, with English abstr.).

Baer, G. and Reches, Z., 1987. Flow patterns of magma in dikes, Makhtesh Ramon, Israel. Geology, 15: 569–572.

Baer, G., Itamar, A., Zilberfarb, A., Rapaport, M. and Vulkan, U., 1985. Subsurface prospecting for base metals in Makhtesh Ramon. Report ZD/106/85, GSI/15/85 (classified).

Bartov, J., 1974. A structural and paleogeographical study of the Central Sinai faults and domes. Ph.D. Diss., Hebrew Univ., Jerusalem, 143 pp. (Hebrew, with English abstr.).

Bentor, Y.K., 1952. Magmatic intrusions and lava-sheets in the Raman area in the Negev (Southern Israel). Geol. Mag., 89: 129–140.

Bentor, Y.K., 1963. The magmatic petrology of Makhtesh Ramon. Proc. Isr. Geol. Soc., 12: 85 pp.

Bentor, Y.K. and Vroman, A.J., 1951. The geological map of the Negev, 1:100,000, sheet 18, (explanatory notes in Hebrew) 98 pp.

Brace, W.F. and Kohlstedt, D.L., 1980. Limits on lithospheric stress imposed by laboratory experiments. J. Geophys. Res., 85: 6248–6252.

De Sitter, L.U., 1962. Structural development of the Arabian shield in Palestine. Geol. Mijnbouw, 41: 116–124.

Dieterich, J.H. and Decker, R.W., 1975. Finite element modeling of surface deformation associated with volcanism. J. Geophys. Res., 80: 4094–4102.

Eyal, Y. and Reches, Z., 1983. Tectonic analysis of the Dead Sea Rift region since the Late-Cretaceous based on mesostructures. Tectonics, 2: 167–185.

Freund, R., 1965. A model of the structural development of Israel and adjacent areas since Upper Cretaceous times. Geol. Mag., 102: 189–205.

Freund, R., Goldberg, M., Weissbrod, T., Druckman, Y. and Derin, B., 1975. The Triassic–Jurassic structure of Israel and its relation to the origin of the eastern Mediterranean. Isr. Geol. Surv. Bull., 65: 26 pp.

Garfunkel, Z., 1964. Tectonic problems along the Ramon lineament. M.Sc. Thesis, Hebrew Univ., Jerusalem, 68 pp. (in Hebrew).

Garfunkel, Z. and Derin, B., 1985. Permian–Early Mesozoic tectonism and continental margin formation in Israel and its implication for the history of the eastern Mediterranean. In: J.E. Dixon and A.H.F. Robertson (Editors), The Geological Evolution of the Eastern Mediterranean. Blackwell, Oxford, pp. 187–201.

Gilbert, G.K., 1877. Report on the geology of the Henry Mountains. U.S. Geographical and Geological Survey, Rocky Mountains Region, 160 pp.

Goldman, M., Steinitz, G., Zafrir, H., Baer, G. and Itamar, A., 1988. The extent and form of the quartz syenite intrusions in the southern Ramon; a TDEM study. Isr. Geol. Soc., Annu. Meet., abstr., p. 39.

Hunt, C.B., 1953. Geology and geography of the Henry Mountains region, Utah. U.S. Geol. Surv., Prof. Pap., 228: 234 pp.

Itamar, A., 1987. Paragenesis and development of hybrid mineral phases in polymetallic vein-type mineralization, Makhtesh Ramon, Israel. Isr. Geol. Soc., Ann. Meet., abstr., p. 63.

Jackson, M.D., 1987. Deformation of host rocks during growth of igneous domes, southern Henry Mountains, Utah. Ph.D. Diss., John Hopkins Univ., Baltimore, Md., 155 pp.

Jackson, M.D. and Pollard, D.D., 1988. The laccolite-stock controversy: New results from the southern Henry Mountains, Utah. Geol. Soc. Am. Bull., 100: 117–139.

Johnson, A.M., 1970. Physical Processes in Geology. Freeman, San Francisco, Calif., 577 pp.

Johnson, A.M. and Page, B.M., 1976. A theory of concentric, kink and sinusoidal folding and of monoclinal flexuring of compressible, elastic multilayers. VII. Development of folds within Huasna syncline, San Luis Obisbo County, California. Tectonophysics, 33: 97–143.

Lang, B. and Steinitz, G., 1985. New K–Ar ages of Mesozoic magmatic rocks in Makhtesh Ramon. Isr. Geol. Soc., Annu. Meet., abstr., pp. 56–57.

Lang, B., Hebeda, E.H., Priem, H.N.A., Steinitz, G. and Verdumen, E.A.Th., 1988. New Rb–Sr age of Early Cretaceous syenites from Makhtesh Ramon and Har Arif. Isr. Geol. Soc., Annu. Meet., abstr., p. 67.

Mazor (Pozner), E., 1955. The magmatic occurrences of Makhtesh Ramon. M.Sc. Thesis, Hebrew Univ., Jerusalem, 29 pp. (in Hebrew).

Mogi, K., 1958. Relations of the eruptions of various volcanoes and the deformations of the ground surfaces around them. Bull. Earthquake Res. Inst. Tokyo Univ., 36: 99–134.

Oppenheimer, D.H., Reasenberg, P.A. and Simpson, R.W., 1988. Fault-plane solutions for the 1984 Morgan Hill, California, earthquake sequence: evidence for the state of stress on the Calaveras Fault. J. Geophys. Res., 93: 9007–9026.

Pollard, D.D., 1968. Deformation of host rocks during sill and laccolith formation. Ph.D. Diss., Stanford Univ., Calif.

Pollard, D.D. and Johnson, A.M., 1973. Mechanics of growth of some laccolithic intrusions in the Henry Mountains, Utah, II. Tectonophysics, 18: 311–354.

Reches, Z., 1987a. Mechanical aspects of pull-apart basins and push-up swells with applications to the Dead Sea transform. Tectonophysics, 141: 75–88.

Reches, Z., 1987b. Determination of the tectonic stress tensor from slip along faults that obey the coulomb yield condition. Tectonics, 6: 849–861.

Reches, Z. and Johnson, A.M., 1978. The development of monoclines, Part II: Mechanical analysis of monoclines. In: V. Matthews (Editor), Laramide Folding Associated with Basement Block Faulting in the Rocky Mountains Region. Geol. Soc. Am., Mem., 151: 278–311.

Ron, H. and Baer, G., 1988. Paleomagnetism of Early Cretaceous rocks from Southern Israel. Isr. J. Earth Sci., 37: 73–81.

Segall, P. and Pollard, D.D., 1980. The mechanics of discontinuous faults. J. Geophys. Res., 85: 4337–4350.

Turner, F.J. and Weiss, L.E., 1963. Structural analysis of metamorphic tectonites. McGraw-Hill, New York, N.Y., 545 pp.

Withjack, M.O. and Scheiner, C., 1982. Fault patterns associated with domes - an experimental and analytical study. Am. Assoc. Pet. Geol. Bull., 66: 302–316.

Zak, I., 1957. The Triassic in Makhtesh Ramon. M.Sc. Thesis, Hebrew Univ., Jerusalem, 84 pp. (in Hebrew).

Zak, I., 1963. Remarks on the stratigraphy and tectonics of the Triassic of Makhtesh Ramon. Isr. J. Earth Sci., 12: 87–89.

Zak, I., 1968. The geological map of Israel, Makhtesh Ramon, Har Gevanim, scale 1 : 20,000. Geol. Survey of Israel.

Zoback, M.D., Zoback, M.L., Mount, V.S., Suppe, J., Eaton, J.P., Healy, J.H., Oppenheimer, D., Reasenberg, P., Jones, L., Raleigh, C.B., Wong, I.G., Scotti, O. and Wentworth, C., 1987. New evidence on the state of stress of the San Andreas Fault System. Science, 238: 1105–1111.